

Precovery Observations of 3I/ATLAS from TESS Suggests Possible Distant Activity

ADINA D. FEINSTEIN  ^{1,*} JOHN W. NOONAN  ² AND DARRYL Z. SELIGMAN  ^{1,†}

¹Department of Physics and Astronomy, Michigan State University, East Lansing, MI 48824, USA

²Department of Physics, Auburn University, Edmund C. Leach Science Center, Auburn, 36849, AL, USA

ABSTRACT

3I/ATLAS is the third macroscopic interstellar object detected traversing the Solar System. Since its initial discovery on UT 01 July 2025, hundreds of hours on a range of observational facilities have been dedicated to measure the physical properties of this object. These observations have provided astrometry to refine the orbital solution, photometry to measure the color, a rotation period and secular light curve, and spectroscopy to characterize the composition of the coma. Here, we report precovery photometry of 3I/ATLAS as observed with NASA’s *Transiting Exoplanet Survey Satellite* (*TESS*). 3I/ATLAS was observed nearly continuously by *TESS* from UT 07 May 2025 to 02 June 2025. We use the shift-stack method to create deep stack images to recover the object. These composite images reveal that 3I/ATLAS has an average *TESS* magnitude of $T_{\text{mag}} = 19.6 \pm 0.1$ and an absolute visual magnitude of $H_V = 12.5 \pm 0.3$, consistent with magnitudes reported in July 2025, suggesting that 3I/ATLAS may have been active out at ~ 6.4 au. Additionally, we extract a ~ 20 day light curve and find no statistically significant evidence of a nucleus rotation period. Nevertheless, the data presented here are some of the earliest precovery images of 3I/ATLAS and may be used in conjunction with future observations to constrain the properties of our third interstellar interloper.

Keywords: Asteroids (72) — Comets (280) — Interstellar Objects (52) — Photometry (1234)

1. INTRODUCTION

Interstellar objects (ISOs) offer unique insights into the formation conditions of rocks and ices in regions of our galaxy beyond the Solar System. The recent discovery of the third ISO, 3I/ATLAS, was reported on UT 01 July 2025 (L. Denneau et al. 2025) by the ATLAS survey (J. L. Tonry et al. 2018a,b). This discovery increases the current census of discovered macroscopic ISOs by 50%. Since its discovery, there has been an international rush to observe 3I/ATLAS before it is no longer visible to observers in February 2026. In particular, early telegrams reported activity in images from the Nordic Optical Telescope (D. Jewitt & J. Luu 2025) and the Two-meter Twin Telescope (M. R. Alarcon et al. 2025). Preliminary reconnaissance observations revealed a reddened reflectance spectrum similar to D-type asteroids, no clear photometric variability and faint cometary activity (T. Karetta et al. 2025; R. de la Fuente Marcos

et al. 2025; C. Opitom et al. 2025; D. Z. Seligman et al. 2025; B. Yang et al. 2025).

Two macroscopic scale ISOs had been discovered before 3I/ATLAS: 1I/‘Oumuamua in 2017 (G. V. Williams et al. 2017) and 2I/Borisov in 2019 (G. Borisov et al. 2019). The light curve of 1I/‘Oumuamua was markedly different from the 3I/ATLAS because it exhibited drastic brightness variations (M. Drabus et al. 2017; W. C. Fraser et al. 2018; M. M. Knight et al. 2017; M. J. S. Belton et al. 2018). This was presumably due to an elongated 6 : 6 : 1 oblate spheroid geometry (S. Mashchenko 2019; A. G. Taylor et al. 2023) and a lack of cometary activity (D. Jewitt et al. 2017; K. J. Meech et al. 2017; Q.-Z. Ye et al. 2017). A significant non-detection of 1I/‘Oumuamua with the *Spitzer* space telescope provided upper limits on the production of carbon-based species (D. E. Trilling et al. 2018). However, 1I/‘Oumuamua had significant radial nongravitational acceleration in its trajectory (M. Micheli et al. 2018). 1I/‘Oumuamua had a reddened color like 3I/ATLAS (M. T. Bannister et al. 2017; A. Fitzsimmons et al. 2018; J. Masiero 2017) and a low velocity at infinity indicating a young kinematic age (E. Gaidos et al. 2017; E. Mamajek 2017). On the contrary, 2I/Borisov dis-

Email: adina@msu.edu

* NASA Sagan Fellow

† NSF Astronomy and Astrophysics Postdoctoral Fellow

played distinct cometary activity (D. Jewitt & J. Luu 2019; A. Fitzsimmons et al. 2019; T. Karetta et al. 2020; C. Opitom et al. 2019; M. T. Bannister et al. 2020; D. Bodewits et al. 2020; G. Cremonese et al. 2020; M. A. Cordiner et al. 2020; P. Guzik et al. 2020; M.-T. Hui et al. 2020; Y. Kim et al. 2020; H. W. Lin et al. 2020; A. J. McKay et al. 2020; Z. Xing et al. 2020; K. Aravind et al. 2021; S. Bagnulo et al. 2021; B. Yang et al. 2021; S. E. Deam et al. 2025). For reviews on ISOs discovered passing through the solar system prior to 3I/ATLAS, we refer the reader to A. Moro-Martín (2022); D. Jewitt & D. Z. Seligman (2023); D. Z. Seligman & A. Moro-Martín (2023); A. Fitzsimmons et al. (2024).

Preccovery observations of small bodies such as comets, asteroids, and ISOs can provide constraints on critical physical properties such as orbit, size, composition, and activity. For example, M.-T. Hui & M. M. Knight (2019) searched for preccovery detections of 1I/‘Oumuamua in Solar and Heliospheric Observatory (SOHO) and Solar TErrestrial RElations Observatory (STEREO) images. Their search provided nondetections, but these nondetections provided critical upper limits on the production rate of dust and water at low heliocentric distances — during a regime of 1I/‘Oumuamua’s trajectory which was entirely unconstrained from extant observations. Q. Ye et al. (2020) reported pre-discovery observations of 2I/Borisov in survey data from the Zwicky Transient Facility (ZTF), as well as a comprehensive search of Catalina Sky Survey and Pan-STARRS data for the object. The combination of preccovery detections and nondetections provided valuable upper limits on the size of the nucleus and information regarding the volatility of ices driving activity. Thus far for 3I/ATLAS, D. Z. Seligman et al. (2025) reported ZTF observations dating back to UT 2025 May 22 and C. O. Chandler et al. (2025) reported observations of using the NSF-DOE Vera C. Rubin Observatory Science Verification (SC) images dating back to UT 2025 June 21. The Rubin Observatory SC observations also revealed faint activity.

All four aforementioned studies highlight the strengths of all-sky surveys in searching for preccovery observations. Although not its original science purpose, NASA’s *Transiting Exoplanet Survey Satellite* (*TESS*; G. R. Ricker et al. 2015) has also been able to recover and discover small bodies in the solar system (A. Pál et al. 2020; G. M. Szabó et al. 2022; C. Kiss et al. 2025) as well as characterize cometary activity (T. L. Farnham et al. 2019, 2021). *TESS* has a large on-sky coverage due to the orientation of four wide-field cameras, where each camera has a field-of-view of $24^\circ \times 24^\circ$, amounting to a total FOV of $96^\circ \times 24^\circ$. These images, known as the *TESS* Full-Frame Images (FFIs), are made avail-

able to the community. *TESS* observes a single field for ~ 27 days, providing a long photometric baseline for variability studies. While limited in its resolution for morphology analysis of cometary comae due to its large pixel scale, *TESS* is excellent for long-term photometric monitoring and analysis.

During the primary mission, *TESS* exclusively observed the northern and southern ecliptic hemispheres. However, in its extended missions, *TESS* was reoriented to observe the ecliptic plane for 10 nonconsecutive sectors. One of these sectors — both fortuitously and serendipitously — happened to observe the exact region where 3I/ATLAS was located. Here, we report the preccovery detection of 3I/ATLAS in the *TESS* Full-Frame Images (FFIs). This manuscript is organized as follows. In Section 2, we present the *TESS* observations and discuss our processing of the FFIs. We present the results of our search in Section 3. We conclude in Section 4. The  icon affiliated with all figures links to the Python script and data used to generate that figure.

2. TESS OBSERVATIONS

TESS re-observed part of the ecliptic plane during Cycle 7 of its second extended mission. Upon discovery of 3I/ATLAS, we used `tess-point` (C. J. Burke et al. 2020) in conjunction with 3I/ATLAS’ best-fit orbital solution from the JPL Horizons Small Bodies Database³ to determine if the object was in the *TESS* FOV. We found that 3I/ATLAS was observed during Sector 92, which occurred from UT 07 May through 03 June 2025.

Each of *TESS*’s four cameras are divided into four charged-coupled devices (CCDs). Due to its high velocity, 3I/ATLAS was observed on two Camera-CCD pairings throughout the sector: Camera 2 CCD 3 and Camera 1 CCD 2. These are located next to each other in the orientation presented in Figure 1. Each *TESS* FFI has an exposure time of 200 seconds. The data is downloaded every ~ 7 days from the spacecraft due to the increased data volume of the higher cadence FFIs. These downlink times occur near apogee and perigee of the orbit of the spacecraft and thereby result in short gaps in the data. The total duration of science data collected during Sector 92 is 26.05 days.

2.1. FFI Selection and Background Removal

We downloaded all FFIs for Camera 2 CCD 3 and Camera 1 CCD 2 using the bulk download scripts provided by the Mikulski Archive for Space Telescopes (MAST)⁴. 3I/ATLAS was observed on pixels $x =$

³ <https://ssd.jpl.nasa.gov/>

⁴ <https://archive.stsci.edu/missions-and-data/tess>

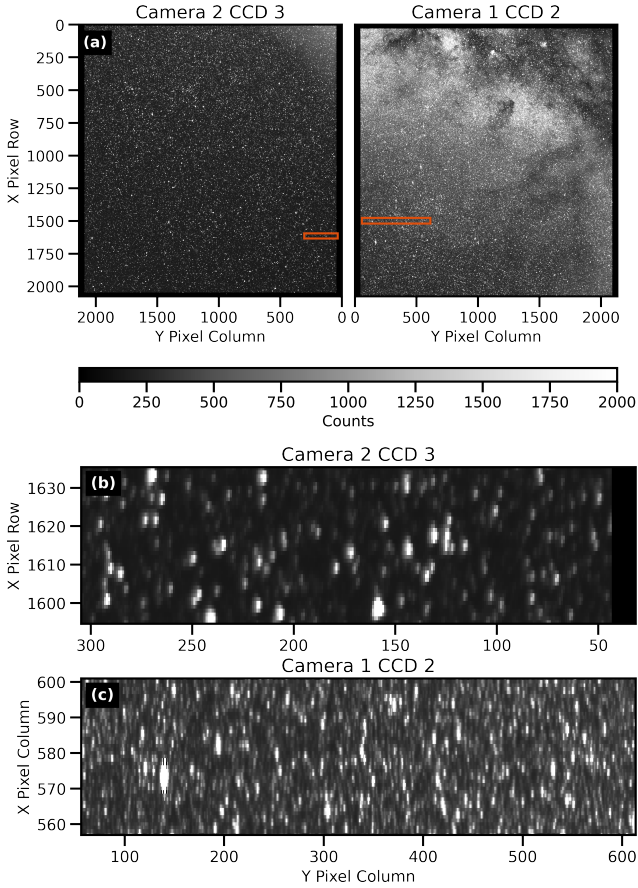


Figure 1. The raw *TESS* FFIs. (a) An example exposure of a full FFI for Camera 2 CCD 3, left, and Camera 1 CCD 2, right. We highlight the region where 3I/ATLAS was observed on both detectors by the orange box. (b) A zoom-in of the field in Camera 2 CCD 3. We note that columns 0 – 44 are serial register columns and are not used in our analysis. (c) A zoom-in of the field in Camera 1 CCD 2. 3I/ATLAS enters a much more crowded field, closer to the ecliptic plane, throughout the sector. All images share the same color scaling. ⚡

[1592, 1635]; $y = [0, 305]$ on Camera 2 CCD 3 and pixels $x = [556, 601]$; $y = [39, 614]$ on Camera 1 CCD 2. We highlight example images of these two regions in Figure 1. It is important to note that columns 0 – 44 are serial register columns, columns 2092 – 2136 are virtual columns, and rows 2048 – 2078 are buffer, smear, and virtual rows; none of these regions can be used for science.

The *TESS* FFIs are contaminated by both zodiacal light and scattered earthshine contamination. In particular, the scattered earthshine manifests as strong ramps at the beginning and end of each *TESS* orbit (~ 13 days). While the background typically varies smoothly, there have been instances of more sporadic and variable behavior (Figure 2). To identify highly con-

taminated FFIs, we calculated the median value in each FFI. The FFIs containing highly non-smooth variability are entirely removed from our analysis (Figure 2). This resulted in the removal of 9% of the available FFIs from Camera 2 CCD and 5% of the available FFIs from Camera 1 CCD 2. In total, after these data-quality cuts, we analyzed 9837 FFIs (353 GB). We provide more specific details pertaining to each Camera/CCD configuration in Table 1.

Once we removed heavily contaminated FFIs, we fit and remove the background from the remaining FFIs. Working with the entire FFI is unnecessary. Instead, we create a “postcard” cutout (A. D. Feinstein et al. 2019) of the entire region where 3I/ATLAS is visible in the FFI (orange boxes in the upper two panels and full bottom two panels in Figure 1). Previous search and recovery analyses of known solar system bodies with *TESS* have fit pixel variability using an n^{th} -order polynomial (e.g. C. Kiss et al. 2025). We choose to model each pixel within the postcard with a data-driven Savistky-Golay filter with a window length of 307 exposures and a 2nd-order polynomial. We opt for this more flexible model as it allows us to accurately model the steep earthshine ramps, without removing any sharp features which may be astrophysical in origin. We explored using smaller and larger window-sizes. We found that smaller window sizes removed astrophysical signals, while larger windows were unable to capture the variability of the orbital ramps.

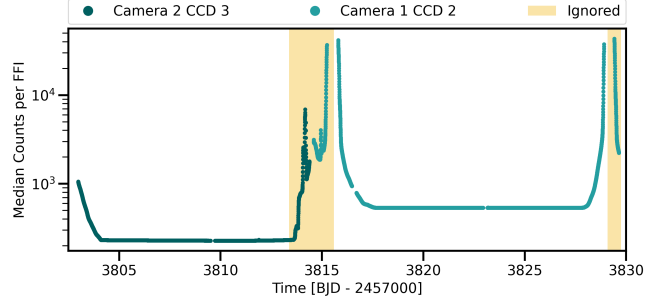


Figure 2. The raw median counts per FFI when 3I/ATLAS is within the FOV. We highlight the strong orbital ramps, gaps, and systematics which were present in Sector 92. We choose to remove FFIs which demonstrated non-smooth variability and/or had unexpected gaps. FFIs which were not used in this analysis are highlighted in yellow. ⚡

2.2. Deep Image Creation

After the background models are removed, we employ a shift-stack algorithm to create a *TESS* deepstack image. We choose not to combine images across detectors, as they may have different systematics. Our algorithm

Table 1. The locations of 3I/ATLAS and corresponding *TESS* Camera/CCD times and pixel locations throughout Sector 92. We denote the number of analyzed FFIs, N_{FFIs} , per Camera/CCD. We note that the *TESS* BJD [TBJD] time is given in units of BJD - 2457000. We denote the heliocentric and geocentric distances as d_{\odot} and d_{\oplus} , respectively.

Camera/ CCD	2/3	1/2
Start [TBJD]	3802.975926	3815.799580
End [TBJD]	3813.474497	3828.911416
Start [UTC]	2025-05-07 11:24:43	2025-05-20 07:10:47
End [UTC]	2025-05-17 23:22:39	2025-06-02 09:51:49
x pixel range	[1592, 1635]	[556, 601]
y pixel range	[0, 305]	[39, 614]
d_{\odot} [au]	6.35 - 5.99	5.92 - 5.47
d_{\oplus} [au]	5.82 - 5.33	5.19 - 4.60
N_{FFI}	4399	5438

works as follows: (I) Query the location of 3I/ATLAS from the JPL Horizons Small Bodies Database for each FFI; (II) Use the world coordinate system information to convert the queried (RA, Dec) to the (x,y) pixel location of 3I/ATLAS; (III) Create a 17×17 pixel cutout around where 3I/ATLAS is expected to be; (IV) Repeat this procedure for all integrations; (V) Sum all of the images. Additionally, due to the apparent location with respect to the galactic plane, we create a data quality flag to track particularly crowded fields. FFIs are flagged when at least 33% of the pixels in the 17×17 cutout are $\geq 2\sigma$ from the median background value. Our methodology works well for objects with known orbital parameters, but is significantly more computationally inefficient when trying to search for new objects. However, it has been employed with some success for example by [W. C. Fraser et al. \(2024\)](#) — albeit using more sensitive data. A coarse summation presented here is sufficient for *TESS* due to its large pixel scale.

We validated our algorithm by recovering another small body which was observed in the same field as 3I/ATLAS. We find that the known main-belt minor planet 896 Sphinx (A918 PE) ($H_V \simeq 15$) was observed on Camera 2 CCD 3. 896 Sphinx was initially discovered in 1918 by M. Wolf. It has a known diameter of 11.9 km ([J. R. Masiero et al. 2014](#)) and rotation period of 21.038 ± 0.008 hours ([T. Polakis 2018](#)). We apply our background-correction and shift-stack method outlined above to the region where 896 Sphinx is within the FFIs.

We present the deepstack image of 896 Sphinx in Figure 3. We find that we are able to recover 896 Sphinx at 6.6σ . Additionally, we extract a light curve using a 3×3 -pixel mask centered on 896 Sphinx. We present

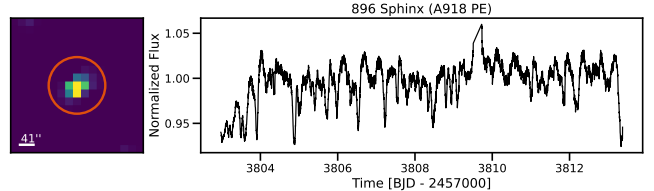


Figure 3. Deepstacked image (left) and light curve (right) of the main belt asteroid 896 Sphinx. We use this object, with an apparent $H = 15$ as a demonstration of our implemented technique to recover 3I/ATLAS. 896 Sphinx has a measured rotation period of ~ 21 hours. Clear variability on a similar timescale can be seen here. These images were stacked from Camera 2 CCD 3. \bullet

the extracted light curve in Figure 3. We find signatures of variability ranging from $\sim 19 - 24$ hours, which is consistent with the known rotation period ([T. Polakis 2018](#)). We note that our algorithm takes ~ 8 minutes to recover this object.

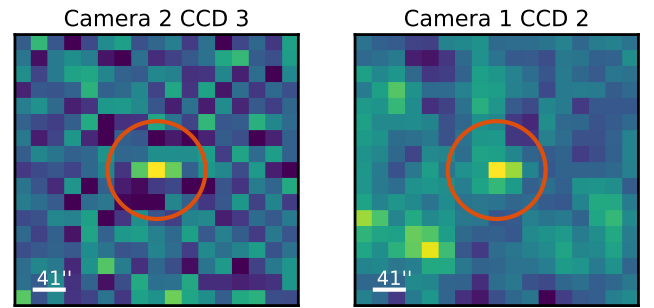


Figure 4. Deepstacked images of 3I/ATLAS in the *TESS* FFIs. We present two images per each camera/CCD pairing. 3I/ATLAS is centered in each image and is highlighted with a red circle. We stack all available FFIs for Camera 2 CCD 3. We limit the stacked images for Camera 1 CCD 2 to cutouts which are not overcrowded with bright sources. Due to the large pixel scale of *TESS* (bottom left), we are unable to resolve any astrometric information from the images. \bullet

We present the two deepstack images of 3I/ATLAS as observed by *TESS* in Figure 4. We stack all available FFIs for Camera 2 CCD 3. We mask the neighboring one pixel around 3I/ATLAS and calculate the median and standard deviation of the background. We find that we are able to detect 3I/ATLAS at 3.7σ above the median background. We do not stack all available FFIs for Camera 1 CCD 2, as the field becomes increasingly more crowded as 3I/ATLAS' apparent motion places it closer to the galactic plane. We use our data quality flag and only use frames that are not significantly contaminated with nearby stars. We stacked 2518 exposures to produce this image (Figure 4, right). We repeat the same significance test and find that we detect

3I/ATLAS at 4.1σ with respect to the median background. Both images represent statistically significant detects of 3I/ATLAS in the *TESS* FFIs.

3. RESULTS

3I/ATLAS has displayed visible cometary activity months prior to perihelion. It is feasible that the level of activity has changed and will continue to change throughout its orbit. Light curves from images when 3I/ATLAS was at further heliocentric distances could provide insights into variations in the activity and nucleus properties such as the rotation period. In this section, we therefore extract the 20-day *TESS* light curve and calculate the resulting secular light curve of 3I/ATLAS.

3.1. Photometric Light Curve

We use a 1-pixel aperture to extract a *TESS* light curve for 3I/ATLAS. Additionally, we create a running-median light curve with a bin width of $n = 11$, which roughly corresponds to 36 minutes in each bin. We convert our light curve from $e^- s^{-1}$ to *TESS* magnitude, T_{mag} using the following relationship:

$$T_{\text{mag}} = -2.5 \log_{10}(c) + 20.44. \quad (1)$$

In Equation 1, c is the number of counts per second. This conversion is provided in the *TESS* Instrumental Handbook (R. Vanderspek et al. 2018). It is important to note that the zero-point has an uncertainty of 0.05 mag. 3I/ATLAS has a $T_{\text{mag}} = 19.6 \pm 0.1$ in the Camera 2 CCD 3 image and a $T_{\text{mag}} = 19.5 \pm 0.1$ in the Camera 1 CCD 2 image. From geometric effects alone, and ignoring the small ($\sim 2.5^\circ$) phase angle change, we would expect the flux from 3I to increase by a factor of 1.5. Converting this back into magnitudes we expected 3I/ATLAS to have a measured magnitude of 19.9 in the Camera 1 CCD 2 images. Within our uncertainty on the magnitude, our observations are statistically inconsistent with an asteroid-like reflectance model that ignores dust production.

These two magnitudes are averaged over the two observing windows in Table 1, which span a range in heliocentric distance of 6.4 to 5.4 au, respectively. In that same time period the distance between 3I/ATLAS and the *TESS* spacecraft decreased by 0.9 au. The rapid change in both these properties can be used to constrain any changes to the overall activity of 3I/ATLAS between the two time periods by investigating if the measured 0.1 mag decrease is consistent with the expected change from both the decreased heliocentric and *TESS* distances.

We convert our light curves into T_{mag} by multiplying the normalized light curve by the average magnitude and analyze our median light curve with a Lomb-Scargle periodogram (N. R. Lomb 1976; J. D. Scargle 1982) to search for evidence of periodicity. We do this for each light curve independently. We search for a rotation period between $P_{\text{rot}} = 1 - 70$ hours, which is mostly consistent with P_{rot} of other kilometer scale small bodies in the solar system (B. D. Warner et al. 2009). Both of the light curves and affiliated periodograms are presented in Figure 5.

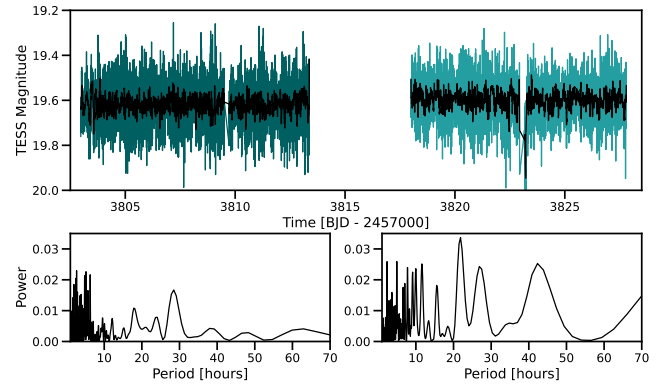


Figure 5. Compiled *TESS* light curve of 3I/ATLAS. We scale the light curve by the calculated T_{mag} from the deep-stacked image (top, colored). We create a binned median light curve with a bin-width of 11 (~ 36 minutes) in black. The *TESS* images offer an advantage when trying to measure the nucleus' rotation period, as 3I/ATLAS was farther from perihelion. We run the binned light curve through a Lomb-Scargle periodogram (bottom panels). We find that while there is a similar peak at ~ 28 hours in both images, there is no strong evidence of a rotation period from the *TESS* images. \bullet

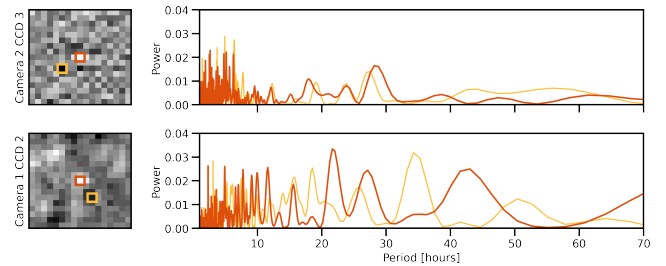


Figure 6. Comparison of the Lomb-Scargle periodogram for 3I/ATLAS (orange) and a background pixel (yellow). We find that the observed peak around ~ 28 hours in the 3I/ATLAS light curve is consistent with background pixels. We find that the light curve and resulting periodogram are dominated by noise and therefore we cannot constrain the rotation period of the nucleus. \bullet

There are several similarities between the Lomb-Scargle periodograms. First, we find that $P_{\text{rot}} < 10$ hours are dominated by noise and/or unremoved systematics. Second, we see that there is no agreement between periodograms at $P > 40$ hours. Third, we see a peak at ~ 28 hours in both periodograms. Although the peaks in the periodograms are offset by 1.3 hours, the similar signal from both detectors could be promising evidence of a rotation period. If $P_{\text{rot}} = 27.65 \pm 0.65$ hours, this would be 16σ discrepant from the current reported period of $P_{\text{rot}} = 16.79 \pm 0.23$ hours (R. de la Fuente Marcos et al. 2025).

To further assess this potential rotational signature, we run the same Lomb-Scargle test for a nearby background pixel in the FFI. Because the background can rapidly vary across the *TESS* detector, we select an example background pixel within 5-pixels of 3I/ATLAS. The results of this test are presented in Figure 6. We find that the background pixel periodograms show a similar peak at $P_{\text{rot}} \simeq 27$ hours. The background pixel peaks are offset from the 3I/ATLAS peaks by 1.3 and 1.6 hours in each image, respectively. Therefore, these *TESS* light curves do not definitively capture a P_{rot} from the nucleus. This may be due to ongoing outgassing even at large heliocentric distances or due to the sensitivity of *TESS*, making any possible magnitude changes from the baseline difficult to definitively measure.

3.2. Secular Light Curve

We calculated the inferred absolute V magnitude of 3I/ATLAS from these observations to add to the light curve presented in D. Z. Seligman et al. (2025). The secular light curve of a comet provides insight into the type of volatile driving activity — or at least the volatility of the species driving activity. For example, M. Womack et al. (2021) presented a 4 year secular light curve of C/1995 O1 (Hale-Bopp) to infer that CO was responsible for the activity exterior to 2.6–3.0 au, while H₂O was responsible for it interior to that.

We convert the calculated *TESS* magnitude to absolute V magnitude, H_V , using the following. T. L. Farnham et al. (2021) derived a rough relationship between the apparent visual magnitude, V , and *TESS* magnitude of

$$V = T_{\text{mag}} + 0.8. \quad (2)$$

This relationship was derived using the Web *TESS* Viewing Tool assuming typical comet colors derived from the average of several Jupiter Family comets, long-period comets, and active centaurs. This relationship has an uncertainty of ± 0.3 mag, which is dominated by

the uncertainty in comet colors. We convert V to H_V using the following:

$$H_V = V - 2.5 n \log_{10}(d_{\odot}) - 5 \log_{10}(d_{\oplus}). \quad (3)$$

In Equation 3, d_{\odot} is the comet-Sun distance, d_{\oplus} is the comet-Earth distance, and n is an activity index. n has a typical range from $n = 2 - 6$, where $n = 2$ assumes the body is inactive and $n = 6$ assumes the object has strong activity (E. Everhart 1967). Given that 3I/ATLAS is at a distance of 6.4 au in these images, we assume $n = 2$.

We use the average d_{\odot} and d_{\oplus} for each Camera/CCD configuration presented in Table 1. From our calculated *TESS* magnitude, following Equations 2 and 3, and adopting the uncertainty presented in T. L. Farnham et al. (2021), we derive $H_V = 12.4 \pm 0.3$ and 12.6 ± 0.3 . We plot discovery and precovery ZTF observations of 3I/ATLAS in Figure 7.

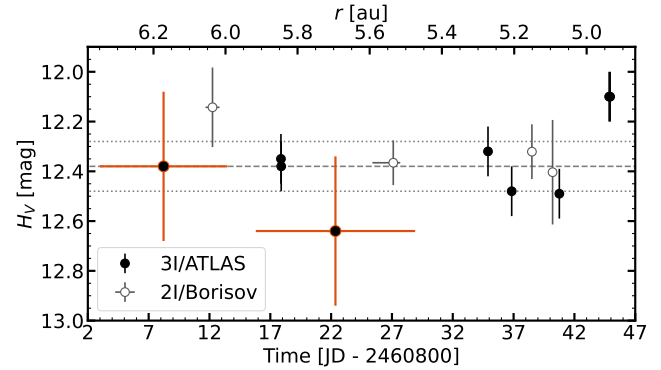


Figure 7. Absolute visual magnitude, H_V computed from *TESS* (orange) and ZTF observations of 3I/ATLAS (black) as compared to 2I/Borisov (gray). The median and 1σ standard deviations of the ZTF observations are plotted as dashed and dotted lines, respectively. The top axes represents the heliocentric distance of 3I/ATLAS and 2I/Borisov at the time of the observation. ZTF observations of 3I/ATLAS were derived in D. Z. Seligman et al. (2025); pre-perihelion observations of 2I/Borisov were derived in Q. Ye et al. (2020).

4. DISCUSSION

We present two deepstack images and a 20-day light curve of 3I/ATLAS as observed with NASA’s *Transiting Exoplanet Survey Satellite*. These data were obtained from 07 May to 03 June 2025, predating the initial discovery by nearly two months (L. Denneau et al. 2025). From these data we calculate that 3I/ATLAS had a $T_{\text{mag}} = 19.6 \pm 0.1$, which is consistent with more recently obtained R_C observations from the TRAPPIST-North and TRAPPIST-South telescopes (D. Z. Seligman

et al. 2025). Moreover, we identify a consistent and periodic signal between both images at ~ 28 hours. However, we find no statistically significant evidence of a rotation period from the nucleus when comparing the light curve of 3I/ATLAS to a neighboring background pixel. The lack of observed rotation may be due to the presence of a coma, uncertainties in the size of the nucleus if there is no coma, or decreased sensitivity of *TESS* to faint objects.

There is no evidence for significant changes to the absolute magnitude of 3I/ATLAS during these observations, at least within the sensitivity limits of the data. It is worth noting that the object traversed nearly 1 au during the course of these observations. This provides tentative evidence that 3I/ATLAS was active during the fortuitous *TESS* observations *prior* to its discovery on UT 01 July 2025. However, the 3σ error technically permits the possibility that 3I/ATLAS was fainter by ~ 1 magnitude during these observations. This is due to the uncertainties in the conversion from T_{mag} magnitudes to V of 0.3 (R. Vanderspek et al. 2018; T. L. Farnham et al. 2021). Therefore, we conclude that these observations are consistent with the hypothesis that 3I/ATLAS was weakly active prior to its discovery. Future work could include deriving a new relationship between T_{mag} and other bandpasses for ISOs.

This distant activity of 3I/ATLAS — if confirmed — could be indicative of mass loss driven by a mechanism other than the sublimation of H₂O ice. One possibility is that 3I/ATLAS is enriched in hypervolatiles such as CO or CO₂. 2I/Borisov displayed a higher production of CO than H₂O when these two quantities were measured contemporaneously (D. Bodewits et al. 2020; M. A. Cordiner et al. 2020; Z. Xing et al. 2020), although no direct measurement of CO₂ has been successfully obtained in an interstellar object to date.⁵ It is also possible that this activity is driven by a more exotic hypervolatile such as H₂ or N₂. The nongravitational acceleration of 1I/‘Oumuamua energetically would have required the sublimation of an ice more volatile than H₂O (Z. Sekanina 2019; D. Seligman & G. Laughlin 2020). It has therefore been proposed that this acceleration was driven by outgassing of N₂ (A. P. Jackson & S. J. Desch 2021), CO (D. Z. Seligman et al. 2021), or radiolytically produced H₂ (J. B. Bergner & D. Z. Seligman 2023). It is possible that distant activity of 3I/ATLAS is driven by one of these, but determining which neutral is responsible requires spectroscopic confirmation or long-term lightcurve modeling (E. Bufanda et al. 2023).

⁵ Production rates of CO₂ have been inferred from the ratio of O I emission features in the visible, A. McKay et al. 2024

The relative flatness of the light curves could be interpreted to indicate very slow changes to the activity rate, which is likely due to the rapidly changing thermal environment of the object. Continued searches for precovery images and extensive monitoring of 3I/ATLAS prior to perihelion will be essential for characterizing this trend. Moreover, spectroscopic follow-up observations could also confirm the existence of hypervolatiles in 3I/ATLAS. Of particular interest in the precovery images would be any stellar occultations or appulses that may exist in the dataset (J. L. Ortiz et al. 2023; C. L. Pereira et al. 2025), especially from multi-filter observatories that could constrain coma densities and composition.

Observations of future ISOs could also shed light on the extent to which this population displays distant activity and is enriched with hypervolatiles. Existing all-sky surveys, including the new Rubin Observatory Legacy Survey of Space and Time (LSST) have been predicted to detect future ISOs (A. Moro-Martín et al. 2009; T. Engelhardt et al. 2017; N. V. Cook et al. 2016; D. Seligman & G. Laughlin 2018; D. J. Hoover et al. 2022; D. Miller et al. 2022; D. Landau et al. 2023; D. Marčeta 2023; D. Marčeta & D. Z. Seligman 2023; R. C. Dorsey et al. 2025). Reorienting *TESS* to observe the ecliptic for longer periods of time in future extended missions could aid in the precovery observations of newly detected ISOs.

5. DATA AND SOFTWARE AVAILABILITY

The raw *TESS* FFIs are available for bulk download on the Mikulski Archive for Space Telescopes.⁶ All of the analysis Python scripts, data behind the figures, and Python scripts for reproducing the figures presented here are available on GitHub.⁷ Additional, larger, data products will be made available on Zenodo upon publication.

This work made use of the following open-source Python packages: `astropy` (Astropy Collaboration et al. 2013, 2018, 2022), `numpy` (S. Van Der Walt et al. 2011), `scipy` (P. Virtanen et al. 2020), `matplotlib` (J. D. Hunter et al. 2007).

6. ACKNOWLEDGMENTS

We thank Henry Hsieh, Davide Farnocchia, and Marco Micheli for thoughtful insights. A.D.F. acknowledges funding from NASA through the NASA Hubble Fellowship grant HST-HF2-51530.001-A awarded by STScI. D.Z.S. is supported by an NSF Astronomy and As-

⁶ https://archive.stsci.edu/tess/bulk_downloads/bulk_downloads_ffi_tp_lc-dv.html

⁷ <https://github.com/afeinstein20/atlas-tess>

trophysics Postdoctoral Fellowship under award AST-2303553. This research award is partially funded by a generous gift of Charles Simonyi to the NSF Division of Astronomical Sciences. The award is made in recognition of significant contributions to Rubin Observatory's Legacy Survey of Space and Time.

7. AUTHOR CONTRIBUTIONS

A.D.F. lead the *TESS* data reduction, the creation of the deepstack images, the light curve extraction, manuscript writing, and figure creation. J.W.N. contributed manuscript text and review. D.Z.S. contributed manuscript text and review.

REFERENCES

- Alarcon, M. R., Serra-Ricart, M., Licandro, J., et al. 2025, Deep g'-band Imaging of Interstellar Comet 3I/ATLAS from the Two-meter Twin Telescope (TTT), *The Astronomer's Telegram*, No. 17264
<https://www.astronomerstelegram.org/?read=17264>
- Aravind, K., Ganesh, S., Venkataramani, K., et al. 2021, *MNRAS*, 502, 3491, doi: [10.1093/mnras/stab084](https://doi.org/10.1093/mnras/stab084)
- Astropy Collaboration, Robitaille, T. P., Tollerud, E. J., et al. 2013, *A&A*, 558, A33, doi: [10.1051/0004-6361/201322068](https://doi.org/10.1051/0004-6361/201322068)
- Astropy Collaboration, Price-Whelan, A. M., Sipőcz, B. M., et al. 2018, *AJ*, 156, 123, doi: [10.3847/1538-3881/aabc4f](https://doi.org/10.3847/1538-3881/aabc4f)
- Astropy Collaboration, Price-Whelan, A. M., Lim, P. L., et al. 2022, *ApJ*, 935, 167, doi: [10.3847/1538-4357/ac7c74](https://doi.org/10.3847/1538-4357/ac7c74)
- Bagnulo, S., Cellino, A., Kolokolova, L., et al. 2021, *Nature Communications*, 12, 1797, doi: [10.1038/s41467-021-22000-x](https://doi.org/10.1038/s41467-021-22000-x)
- Bannister, M. T., Schwamb, M. E., Fraser, W. C., et al. 2017, *ApJL*, 851, L38, doi: [10.3847/2041-8213/aaa07c](https://doi.org/10.3847/2041-8213/aaa07c)
- Bannister, M. T., Opitom, C., Fitzsimmons, A., et al. 2020, arXiv e-prints, arXiv:2001.11605.
<https://arxiv.org/abs/2001.11605>
- Belton, M. J. S., Hainaut, O. R., Meech, K. J., et al. 2018, *ApJL*, 856, L21, doi: [10.3847/2041-8213/aab370](https://doi.org/10.3847/2041-8213/aab370)
- Bergner, J. B., & Seligman, D. Z. 2023, *Nature*, 615, 610, doi: [10.1038/s41586-022-05687-w](https://doi.org/10.1038/s41586-022-05687-w)
- Bodewits, D., Noonan, J. W., Feldman, P. D., et al. 2020, *Nature Astronomy*, 4, 867, doi: [10.1038/s41550-020-1095-2](https://doi.org/10.1038/s41550-020-1095-2)
- Borisov, G., Durig, D. T., Sato, H., et al. 2019, *Central Bureau Electronic Telegrams*, 4666, 1
- Bufanda, E., Meech, K., Kleyna, J., Keane, J., & Hainaut, O. 2023, in *AAS/Division for Planetary Sciences Meeting Abstracts*, Vol. 55, *AAS/Division for Planetary Sciences Meeting Abstracts* #55, 400.09
- Burke, C. J., Levine, A., Fausnaugh, M., et al. 2020, *TESS-Point: High precision TESS pointing tool*, *Astrophysics Source Code Library*, record ascl:2003.001
- Chandler, C. O., Bernardinelli, P. H., Jurić, M., et al. 2025, arXiv e-prints, arXiv:2507.13409, doi: [10.48550/arXiv.2507.13409](https://doi.org/10.48550/arXiv.2507.13409)
- Cook, N. V., Ragazzine, D., Granvik, M., & Stephens, D. C. 2016, *ApJ*, 825, 51, doi: [10.3847/0004-637X/825/1/51](https://doi.org/10.3847/0004-637X/825/1/51)
- Cordiner, M. A., Milam, S. N., Biver, N., et al. 2020, *Nature Astronomy*, 4, 861, doi: [10.1038/s41550-020-1087-2](https://doi.org/10.1038/s41550-020-1087-2)
- Cremonese, G., Fulle, M., Cambianica, P., et al. 2020, *ApJL*, 893, L12, doi: [10.3847/2041-8213/ab8455](https://doi.org/10.3847/2041-8213/ab8455)
- de la Fuente Marcos, R., Licandro, J., Alarcon, M. R., et al. 2025, arXiv e-prints, arXiv:2507.12922.
<https://arxiv.org/abs/2507.12922>
- Deam, S. E., Bannister, M. T., Opitom, C., et al. 2025, arXiv e-prints, arXiv:2507.05051, doi: [10.48550/arXiv.2507.05051](https://doi.org/10.48550/arXiv.2507.05051)
- Denneau, L., Siverd, R., Tonry, J., et al. 2025, *MPEC*
- Dorsey, R. C., Hopkins, M. J., Bannister, M. T., et al. 2025, arXiv e-prints, arXiv:2502.16741, doi: [10.48550/arXiv.2502.16741](https://doi.org/10.48550/arXiv.2502.16741)
- Drahus, M., Yang, B., Lis, D. C., & Jewitt, D. 2017, *MNRAS*, 468, 2897, doi: [10.1093/mnras/stw2227](https://doi.org/10.1093/mnras/stw2227)
- Engelhardt, T., Jedicke, R., Vereš, P., et al. 2017, *Astronomical Journal*, 153, 133, doi: [10.3847/1538-3881/aa5c8a](https://doi.org/10.3847/1538-3881/aa5c8a)
- Everhart, E. 1967, *AJ*, 72, 716, doi: [10.1086/110299](https://doi.org/10.1086/110299)
- Farnham, T. L., Kelley, M. S. P., & Bauer, J. M. 2021, *PSJ*, 2, 236, doi: [10.3847/PSJ/ac323d](https://doi.org/10.3847/PSJ/ac323d)
- Farnham, T. L., Kelley, M. S. P., Knight, M. M., & Feaga, L. M. 2019, *ApJL*, 886, L24, doi: [10.3847/2041-8213/ab564d](https://doi.org/10.3847/2041-8213/ab564d)
- Feinstein, A. D., Montet, B. T., Foreman-Mackey, D., et al. 2019, *PASP*, 131, 094502, doi: [10.1088/1538-3873/ab291c](https://doi.org/10.1088/1538-3873/ab291c)
- Fitzsimmons, A., Meech, K., Matrà, L., & Pfalzner, S. 2024, in *Comets III*, ed. K. J. Meech, M. R. Combi, D. Bockelée-Morvan, S. N. Raymond, & M. E. Zolensky, 731–766
- Fitzsimmons, A., Snodgrass, C., Rozitis, B., et al. 2018, *Nature Astronomy*, 2, 133, doi: [10.1038/s41550-017-0361-4](https://doi.org/10.1038/s41550-017-0361-4)
- Fitzsimmons, A., Hainaut, O., Meech, K. J., et al. 2019, *ApJL*, 885, L9, doi: [10.3847/2041-8213/ab49fc](https://doi.org/10.3847/2041-8213/ab49fc)
- Fraser, W. C., Pravec, P., Fitzsimmons, A., et al. 2018, *Nature Astronomy*, 2, 383, doi: [10.1038/s41550-018-0398-z](https://doi.org/10.1038/s41550-018-0398-z)

- Fraser, W. C., Porter, S. B., Peltier, L., et al. 2024, PSJ, 5, 227, doi: [10.3847/PSJ/ad6f9e](https://doi.org/10.3847/PSJ/ad6f9e)
- Gaidos, E., Williams, J., & Kraus, A. 2017, RNAAS, 1, 13, doi: [10.3847/2515-5172/aa9851](https://doi.org/10.3847/2515-5172/aa9851)
- Guzik, P., Drahus, M., Rusek, K., et al. 2020, Nature Astronomy, 4, 53, doi: [10.1038/s41550-019-0931-8](https://doi.org/10.1038/s41550-019-0931-8)
- Hoover, D. J., Seligman, D. Z., & Payne, M. J. 2022, Planetary Science Journal, 3, 71, doi: [10.3847/PSJ/ac58fe](https://doi.org/10.3847/PSJ/ac58fe)
- Hui, M.-T., & Knight, M. M. 2019, AJ, 158, 256, doi: [10.3847/1538-3881/ab50b8](https://doi.org/10.3847/1538-3881/ab50b8)
- Hui, M.-T., Ye, Q.-Z., Föhring, D., Hung, D., & Tholen, D. J. 2020, AJ, 160, 92, doi: [10.3847/1538-3881/ab9df8](https://doi.org/10.3847/1538-3881/ab9df8)
- Hunter, J. D., et al. 2007, Computing in science and engineering, 9, 90
- Jackson, A. P., & Desch, S. J. 2021, Journal of Geophysical Research (Planets), 126, e06706, doi: [10.1029/2020JE006706](https://doi.org/10.1029/2020JE006706)
- Jewitt, D., & Luu, J. 2019, ApJL, 886, L29, doi: [10.3847/2041-8213/ab530b](https://doi.org/10.3847/2041-8213/ab530b)
- Jewitt, D., & Luu, J. 2025, Interstellar Interloper C/2025 N1 is Active,, The Astronomer's Telegram, No. 17263 <https://www.astronomerstelegram.org/?read=17263>
- Jewitt, D., Luu, J., Rajagopal, J., et al. 2017, Astrophysical Journal Letters, 850, L36, doi: [10.3847/2041-8213/aa9b2f](https://doi.org/10.3847/2041-8213/aa9b2f)
- Jewitt, D., & Seligman, D. Z. 2023, ARA&A, 61, 197, doi: [10.1146/annurev-astro-071221-054221](https://doi.org/10.1146/annurev-astro-071221-054221)
- Kareta, T., Andrews, J., Noonan, J. W., et al. 2020, ApJL, 889, L38, doi: [10.3847/2041-8213/ab6a08](https://doi.org/10.3847/2041-8213/ab6a08)
- Kareta, T., Champagne, C., McClure, L., et al. 2025, arXiv e-prints, arXiv:2507.12234. <https://arxiv.org/abs/2507.12234>
- Kim, Y., Jewitt, D., Mutchler, M., et al. 2020, ApJL, 895, L34, doi: [10.3847/2041-8213/ab9228](https://doi.org/10.3847/2041-8213/ab9228)
- Kiss, C., Takács, N., Kalup, C. E., et al. 2025, A&A, 694, L17, doi: [10.1051/0004-6361/202453509](https://doi.org/10.1051/0004-6361/202453509)
- Knight, M. M., Protopapa, S., Kelley, M. S. P., et al. 2017, Astrophysical Journal Letters, 851, L31, doi: [10.3847/2041-8213/aa9d81](https://doi.org/10.3847/2041-8213/aa9d81)
- Landau, D., Donitz, B., & Karimi, R. 2023, Acta Astronautica, 206, 133, doi: [10.1016/j.actaastro.2023.02.021](https://doi.org/10.1016/j.actaastro.2023.02.021)
- Lin, H. W., Lee, C.-H., Gerdes, D. W., et al. 2020, ApJL, 889, L30, doi: [10.3847/2041-8213/ab6bd9](https://doi.org/10.3847/2041-8213/ab6bd9)
- Lomb, N. R. 1976, Ap&SS, 39, 447, doi: [10.1007/BF00648343](https://doi.org/10.1007/BF00648343)
- Mamajek, E. 2017, Research Notes of the American Astronomical Society, 1, 21, doi: [10.3847/2515-5172/aa9bdc](https://doi.org/10.3847/2515-5172/aa9bdc)
- Marčeta, D. 2023, Astronomy and Computing, 42, 100690, doi: [10.1016/j.ascom.2023.100690](https://doi.org/10.1016/j.ascom.2023.100690)
- Marčeta, D., & Seligman, D. Z. 2023, Planetary Science Journal, 4, 230, doi: [10.3847/PSJ/ad08c1](https://doi.org/10.3847/PSJ/ad08c1)
- Mashchenko, S. 2019, MNRAS, 489, 3003, doi: [10.1093/mnras/stz2380](https://doi.org/10.1093/mnras/stz2380)
- Masiero, J. 2017, arXiv e-prints, arXiv:1710.09977. <https://arxiv.org/abs/1710.09977>
- Masiero, J. R., Grav, T., Mainzer, A. K., et al. 2014, ApJ, 791, 121, doi: [10.1088/0004-637X/791/2/121](https://doi.org/10.1088/0004-637X/791/2/121)
- McKay, A., Opitom, C., Jehin, E., et al. 2024, in AAS/Division for Planetary Sciences Meeting Abstracts, Vol. 56, 56th Annual Meeting of the Division for Planetary Sciences, 301.01
- McKay, A. J., Cochran, A. L., Dello Russo, N., & DiSanti, M. A. 2020, ApJL, 889, L10, doi: [10.3847/2041-8213/ab64ed](https://doi.org/10.3847/2041-8213/ab64ed)
- Meech, K. J., Weryk, R., Micheli, M., et al. 2017, Nature, 552, 378, doi: [10.1038/nature25020](https://doi.org/10.1038/nature25020)
- Micheli, M., Farnocchia, D., Meech, K. J., et al. 2018, Nature, 559, 223, doi: [10.1038/s41586-018-0254-4](https://doi.org/10.1038/s41586-018-0254-4)
- Miller, D., Duvigneaud, F., Menken, W., Landau, D., & Linares, R. 2022, Acta Astronautica, 200, 242, doi: [10.1016/j.actaastro.2022.07.053](https://doi.org/10.1016/j.actaastro.2022.07.053)
- Moro-Martín, A. 2022, arXiv e-prints, arXiv:2205.04277, doi: [10.48550/arXiv.2205.04277](https://doi.org/10.48550/arXiv.2205.04277)
- Moro-Martín, A., Turner, E. L., & Loeb, A. 2009, Astrophysical Journal, 704, 733, doi: [10.1088/0004-637X/704/1/733](https://doi.org/10.1088/0004-637X/704/1/733)
- Opitom, C., Fitzsimmons, A., Jehin, E., et al. 2019, A&A, 631, L8, doi: [10.1051/0004-6361/201936959](https://doi.org/10.1051/0004-6361/201936959)
- Opitom, C., Snodgrass, C., Jehin, E., et al. 2025, Initial VLT/MUSE spectroscopy of the interstellar object 3I/ATLAS, <https://arxiv.org/abs/2507.05226>
- Ortiz, J. L., Pereira, C. L., Sicardy, B., et al. 2023, A&A, 676, L12, doi: [10.1051/0004-6361/202347025](https://doi.org/10.1051/0004-6361/202347025)
- Pál, A., Szakáts, R., Kiss, C., et al. 2020, ApJS, 247, 26, doi: [10.3847/1538-4365/ab64f0](https://doi.org/10.3847/1538-4365/ab64f0)
- Pereira, C. L., Braga-Ribas, F., Sicardy, B., et al. 2025, Philosophical Transactions of the Royal Society of London Series A, 383, 20240189, doi: [10.1098/rsta.2024.0189](https://doi.org/10.1098/rsta.2024.0189)
- Polakis, T. 2018, Minor Planet Bulletin, 45, 347
- Ricker, G. R., Winn, J. N., Vanderspek, R., et al. 2015, Journal of Astronomical Telescopes, Instruments, and Systems, 1, 014003, doi: [10.1117/1.JATIS.1.1.014003](https://doi.org/10.1117/1.JATIS.1.1.014003)
- Scargle, J. D. 1982, ApJ, 263, 835, doi: [10.1086/160554](https://doi.org/10.1086/160554)
- Sekanina, Z. 2019, arXiv e-prints, arXiv:1905.00935, doi: [10.48550/arXiv.1905.00935](https://doi.org/10.48550/arXiv.1905.00935)
- Seligman, D., & Laughlin, G. 2018, AJ, 155, 217, doi: [10.3847/1538-3881/aabd37](https://doi.org/10.3847/1538-3881/aabd37)

- Seligman, D., & Laughlin, G. 2020, ApJL, 896, L8, doi: [10.3847/2041-8213/ab963f](https://doi.org/10.3847/2041-8213/ab963f)
- Seligman, D. Z., Levine, W. G., Cabot, S. H. C., Laughlin, G., & Meech, K. 2021, ApJ, 920, 28, doi: [10.3847/1538-4357/ac1594](https://doi.org/10.3847/1538-4357/ac1594)
- Seligman, D. Z., & Moro-Martín, A. 2023, Contemporary Physics, 63, 200, doi: [10.1080/00107514.2023.2203976](https://doi.org/10.1080/00107514.2023.2203976)
- Seligman, D. Z., Micheli, M., Farnocchia, D., et al. 2025, arXiv e-prints, arXiv:2507.02757, doi: [10.48550/arXiv.2507.02757](https://doi.org/10.48550/arXiv.2507.02757)
- Szabó, G. M., Pál, A., Szigeti, L., et al. 2022, A&A, 661, A48, doi: [10.1051/0004-6361/202142223](https://doi.org/10.1051/0004-6361/202142223)
- Taylor, A. G., Seligman, D. Z., Hainaut, O. R., & Meech, K. J. 2023, PSJ, 4, 186, doi: [10.3847/PSJ/acf617](https://doi.org/10.3847/PSJ/acf617)
- Tonry, J. L., Denneau, L., Heinze, A. N., et al. 2018a, PASP, 130, 064505, doi: [10.1088/1538-3873/aabadf](https://doi.org/10.1088/1538-3873/aabadf)
- Tonry, J. L., Denneau, L., Flewelling, H., et al. 2018b, ApJ, 867, 105, doi: [10.3847/1538-4357/aae386](https://doi.org/10.3847/1538-4357/aae386)
- Trilling, D. E., Mommert, M., Hora, J. L., et al. 2018, Astronomical Journal, 156, 261
- Van Der Walt, S., Colbert, S. C., & Varoquaux, G. 2011, Computing in Science & Engineering, 13, 22
- Vanderspek, R., Doty, J. P., Fausnaugh, M., et al. 2018, TESS Instrument Handbook, v0.1, Mikulski Archive for Space Telescopes, https://archive.stsci.edu/missions/tess/doc/TESS_Instrument_Handbook_v0.1.pdf
- Virtanen, P., Gommers, R., Oliphant, T. E., et al. 2020, Nature Methods, 17, 261, doi: [10.1038/s41592-019-0686-2](https://doi.org/10.1038/s41592-019-0686-2)
- Warner, B. D., Harris, A. W., & Pravec, P. 2009, Icarus, 202, 134, doi: [10.1016/j.icarus.2009.02.003](https://doi.org/10.1016/j.icarus.2009.02.003)
- Williams, G. V., Sato, H., Sarneczky, K., et al. 2017, Central Bureau Electronic Telegrams, 4450, 1
- Womack, M., Curtis, O., Rabson, D. A., et al. 2021, PSJ, 2, 17, doi: [10.3847/PSJ/abd32c](https://doi.org/10.3847/PSJ/abd32c)
- Xing, Z., Bodewits, D., Noonan, J., & Bannister, M. T. 2020, ApJL, 893, L48, doi: [10.3847/2041-8213/ab86be](https://doi.org/10.3847/2041-8213/ab86be)
- Yang, B., Meech, K. J., Connelley, M., & Keane, J. V. 2025, arXiv e-prints, arXiv:2507.14916, <https://arxiv.org/abs/2507.14916>
- Yang, B., Li, A., Cordiner, M. A., et al. 2021, Nature Astronomy, doi: [10.1038/s41550-021-01336-w](https://doi.org/10.1038/s41550-021-01336-w)
- Ye, Q., Kelley, M. S. P., Bolin, B. T., et al. 2020, AJ, 159, 77, doi: [10.3847/1538-3881/ab659b](https://doi.org/10.3847/1538-3881/ab659b)
- Ye, Q.-Z., Zhang, Q., Kelley, M. S. P., & Brown, P. G. 2017, Astrophysical Journal Letters, 851, L5, doi: [10.3847/2041-8213/aa9a34](https://doi.org/10.3847/2041-8213/aa9a34)